Modelling high velocity impact on thin woven composite plates: A non-dimensional theoretical approach

Citation for published version:
Alonso San Jose, L, Garcia-Gonzalez, D, Martinez-Hergueta, F, Navarro, C, Teixeira-Dias, F & Garca-Castillo, SK 2021, 'Modelling high velocity impact on thin woven composite plates: A non-dimensional theoretical approach', *Mechanics of Advanced Materials and Structures*, pp. 1-23. https://doi.org/10.1080/15376494.2021.1878402

Digital Object Identifier (DOI):
10.1080/15376494.2021.1878402

Link:
Link to publication record in Edinburgh Research Explorer

Document Version:
Peer reviewed version

Published In:
Mechanics of Advanced Materials and Structures

Modelling high velocity impact on thin woven composite plates: A non-dimensional theoretical approach

L. Alonso[a], D. Garcia-Gonzalez[b], F. Martínez-Hergueta[c], C. Navarro[b], F. Teixeira-Dias[c], S.K. García-Castillo[b]

[a]*Department of Chemical Technology, Energy and Mechanics, Rey Juan Carlos University C/Tulipán s.n., 28933*
[b]*Department of Continuum Mechanics and Structural Analysis, University Carlos III of Madrid Avda. de la Universidad 30, Madrid 28911, Spain*
[c]*School of Engineering, IIE — Institute for Infrastructure and Environment, The University of Edinburgh Edinburgh EH9 3FG, United Kingdom*

Abstract

A new theoretical energy-based model that predicts the ballistic behaviour of thin woven composite laminates is presented. This model formulated for high-velocity impacts, where the boundary conditions (applied at the external edges of the impacted plate) do not play a relevant role. This can be assumed as the mechanical waves do not reach the borders during the impact event, being the local structural behaviour the responsible for the ballistic performance. A non-dimensional formulation is used to analyse the influence of material properties and geometrical parameters in the ballistic response of the laminate. The model is physically-based on the energy contribution of different energy-absorption mechanisms. A 3D finite element model previously developed is used to simulate the performance of the laminate under high-velocity impacts and to validate the hypotheses of the theoretical model. A comparison between FE and theoretical models is performed by means of energy absorption mechanisms. For that, the failure modes of the FE model are related to the corresponding energy-absorption mechanisms of the theoretical associated. The evaluation of the theoretical results is straightforward although the FEM results require the evaluation of the energy absorbed by each element that fails under each criterion. The predictive capability of the proposed model is verified against experimental results, which were obtained from previous studies carried out by the authors. The results obtained show the dependencies between the ballistic response and the non-dimensional physical parameters of the model. Furthermore, the proposed model can be used to see the relative importance of the different energy-absorption mechanisms involved and the comparison of these mechanisms between the theoretical and the FE models can reflect the different roles played by them, depending on the material properties and geometrical characteristics of the laminate. These results highlight the relevance of the in-plane energy-absorption mechanisms, which rule the penetration process for thin laminates.

Keywords: Woven composites, Ballistic response, Theoretical modelling, Numerical modelling, Energy-based analysis

1. Introduction

Composite materials are suitable for a large number of lightweight structural applications, namely in transports engineering, where weight reductions, and consequently fuel efficiency, are key priorities (Llorca et al., 2011). Consequently, it is essential to pay attention to the response of these materials under extraordinary circumstances such as impacts that can affect their mechanical properties and compromise their performance. In-plane mechanical properties of composite laminates, however, are known to quickly deteriorate when subjected to out-of-plane impact loads (Alonso et al., 2018b). There are different approaches to tackle the impact phenomenon: experimental, numerical and analytical. Although experimental and finite element approaches are still the preferred methods to study the impact behaviour of composite materials, their use is often limited by high computational costs (Miamí et al., 2007). On the other hand, analytical and theoretical approaches, as shown in this paper, are good alternatives to understand the physics of the problem and provide sufficiently accurate solutions at lower computational cost than numerical methods (Naik and Doshi, 2005).

Most analytical approaches predict the residual velocity through conservation of momentum and energy balances. Models exclusively based on momentum transfer are physically consistent but are limited in providing information on specific energy-absorption mechanisms (Briescani et al., 2015; Mamivand and Liaghat, 2010). Models that include energy balances, however, provide fundamental insights on the different failure mechanisms. This has motivated a formulation based on energy-absorption mechanisms in this study. The level of detail is proportional to the complexity of the mechanisms described by the analytical equations and the initial hypotheses considered. Regarding energy-based theoretical models, the current literature is divided between models for thin and thick laminates. Often, the initial hypotheses considered (behaviour of the laminate, energy-absorption mechanisms considered and neglected) are different depending on the thickness, leading to diverse formulations. In a previous study carried out by the authors (Alonso et al., 2018a), the threshold from which a laminate changes its structural response from thin to thick was found at laminate thickness close to the projectile diameter. Analytical models that can predict the ballistic performance of thin laminates often consider non-spherical projectile geometries and are limited to in-plane failure modes: elastic deformation of fibres, tensile failure of fibres, movement of the laminate, matrix cracking and delamination (Zhu et al., 1992; Navarro, 1998; Moyre et al., 2000; Naik and Shrirao, 2004; García-Castillo et al., 2013). These models have been further extended to predict the response of thick composite plates, incorporating additional energy absorption mechanisms such as shear plugging and crushing while neglecting others (Naik and Shrirao, 2004; Naik and Doshi, 2005; Naik et al., 2005, 2006). A number of different approaches can be found in the literature that also consider the shape of the projectile, observing significant differences in the energy absorption of thick laminates impacted by blunt, conical and truncated projectiles (Wen, 2000, 2001). Nevertheless, studies considering diverse shapes of the projectile when impacting thin laminates do not show remarkable differences in the ballistic response. Regarding thin laminates, further research is required to capture the penetration rate and the relative contribution of each mechanism in the final energy absorption capacity of the laminate.

One of the issues hindering the implementation of more accurate analytical models is the difficulty to introduce new hypotheses, such as the relative displacement between the projectile and the laminate to define the perforation process, which is newly introduced in this paper, to the best of our knowledge, for high-velocity impact models. High-speed cameras do not provide sufficient resolution to ascertain the physical processes in the first instants of the impact event and, therefore, can not be used to validate the contribution of different failure mechanisms (Gellert et al., 2000; Buitrago-Pérez et al., 2010). In this context, numerical modelling is a complementary tool to clarify the micro-mechanisms involved in complex problems such as impact (Moyre et al., 2000; Naik and Doshi, 2005; López-Puente et al., 2007; Briescani et al., 2015; Alonso et al., 2018a). Some authors have combined analytical and numerical models, also using the numerical model as a tool to validate the ballistic results of the analytical. (Mohotti et al., 2015; Gregori et al., 2020) developed analytical models for aluminium–polyurea composite layered plates and ceramic-composite targets respectively and validated them with finite element simulations with the software LS-DYNA.

This work aims at characterising the ballistic response of thin GFRP laminates through theoretical modelling. To this end, a non-dimensional theoretical model is proposed, based on physical energy-based hypotheses. The model provides information about the ballistic behaviour and the energy-absorption mechanisms. The impact vs residual velocity curve is compared with experimental data from the literature (Buitrago-Pérez et al., 2010). The present model incorporates, for the first time, new hypotheses which allow for the prediction of the penetration rate and final indentation in the laminate. Although the analysis focuses on spherical projectiles, the model is formulated so that it accounts for different projectile geometries. Furthermore, a numerical constitutive model for woven composites, previously developed by the authors (Alonso et al., 2020), is used to validate the theoretical assumptions behind the proposed formulation. The model proposes a continuum damage mechanics approach based on a maximum stress criteria. The energy absorbed by the elements that fail under each criterion is related to the corresponding energy-absorption mechanism or a combination of some in the theoretical model. The failure criteria in the FEM as well as the energy-absorption mechanisms in the theoretical model can be classified into in-plane and out-of-plane failure criteria/energy-absorption mechanisms. The proposed analytical model is an efficient tool to evaluate both the ballistic response and transitions in the relative roles played by specific energy-absorption mechanisms, depending on the material properties and geometrical characteristics of the plate. These outcomes are useful to address the first design and optimisation stages of structural components subjected to impact loading.

2. Theoretical model

The energy-based theoretical model developed to predict the ballistic performance of thin woven E-glass/polymer laminates is presented in this section. The model assumes that the kinetic energy of the projectile is partly dissipated during the perforation process and partly transferred to the composite laminate. The model hypotheses, the kinematics of the perforation process and the formulation of the energy absorption mechanisms are described in the following paragraphs.

This model is based on a previous non-dimensional energy-based model that takes into account the same energy-absorption mechanisms but assumes simpler hypotheses (Alonso et al., 2018a). To identify the model parameters, a non-dimensional formulation is used based on the Vaschy-Buckingham Π theorem. The model depends on three elemental magnitudes: the mass [M], length [L] and time [T], which can be written in non-dimensional form as

$$[M] = \rho_p \phi_p^3 \tag{1}$$

$$[L] = \phi_p \tag{2}$$

$$[T] = \frac{\phi_p}{V_i} \tag{3}$$

where ρ_p is the density of the projectile material, ϕ_p is the projectile diameter and V_i is the impact velocity.

The following hypotheses are proposed. Some of them are based on previous experimental observations (Buitrago-Pérez et al. (2010); García-Castillo et al. (2006); Alonso et al. (2018a)):

- The projectile is rigid and, as such, remains undeformed during the impact.
- The laminate has linear-elastic behaviour and is x-axially symmetric (x is the thickness direction).
- Wave speeds do not change during the impact.
- The laminate is accelerated by the projectile.
- During penetration, the laminate moves with a different velocity from that of the projectile. Consequently, there is a relative displacement between the projectile and the laminate.
- The model accounts for the time before the relative displacement between the projectile and the laminate equals the thickness of the laminate. From this moment onward, no further energy transfer is considered.
- The energy dissipated through tensile failure and elastic deformation of the fibres is accounted for separately.
- The energy dissipated by friction, shear plugging and heat transfer is negligible.

As mentioned before, the model is formulated in a non-dimensional way. This formulation leads to the apparition of the parameters defined in Table 1. The dynamic properties at high strain rates, presented in Table 1, used in the theoretical and numerical models are estimated from the static properties obtained in Alonso et al. (2018a, 2020) taking into account the relations proposed by Harding and Welsh (1983); Harding and Ruiz (1998). The high-strain rate correction factors for the failure limits and for the shear and Young's moduli are estimated at 1.5 and 3, respectively. .

Table 1: Summary of the parameters and Π groups of the problem.

Parameter	**Nomenclature**	**Value**	**Π group**
Projectile diameter	ϕ_p	7.5 [mm]	
Projectile density	ρ_p	7809 [kg.m^{-3}]	
Impact velocity	v_i [m.s]		
Laminate thickness	e		$\Pi_e = \frac{e}{\phi_p}$
In-plane Young's modulus	E	15.2 [GPa]	$\Pi_E = \frac{E}{\rho_p {v_i}^2}$
In-plane failure strain	ε_r	0.0725	ε_r
In-plane failure stress	σ_r	1.102 [GPa]	$\Pi_{\sigma_r} = \frac{\sigma_r}{\rho_p {v_i}^2}$
Laminate density	ρ_l	1980 [kg.m^{-3}]	$\Pi_{\rho_l} = \frac{\rho_l}{\rho_p}$
Absorbed energy density by matrix cracking	E_{MT}	10^6 [J.m^{-3}]	$\Pi_{E_{MT}} = \frac{E_{MT}}{\rho_p {v_i}^2}$
Critical dynamic-strain energy-release rate in mode II	G_{IICD}	3000 [J.m^{-2}]	$\Pi_{G_{IICD}} = \frac{G_{IICD}}{\rho_p \phi_p {v_i}^2}$
Yarn width	B	5 [mm]	$\Pi_B = \frac{B}{\phi_p}$
Stress wave transmission factor	b	0.9	b
Poisson's ratio	ν	0.16	$\Pi_\nu = [12(1-\nu^2)]^{1/6}$
Shape factor of delamination	α_{DL}	1	α_{DL}
Shape factor of matrix cracking	α_{MC}	1	α_{MC}
Constant	c	0.25 [N.m]$^{-1/6}$	$\Pi_c = c{\phi_p}^{1/2}{\rho_p}^{1/6}{V_i}^{1/3}$

As shown in Table 1, the parameters combinations which govern the problem can be associated with physical meaning. These combinations are known as the Π groups of the problem. In this model, the mechanics of the impact and penetration depends on 16 fundamental parameters which are listed in Table 1, together with their corresponding Π groups associated with them. In view of Table 1, note that some of the parameters (ε_r, b) are inherently non-dimensional, so the parameter is directly the Π group in those cases. Eventually, after applying the Vaschy-Buckingham Theorem, the problem depends on 13 Π groups.

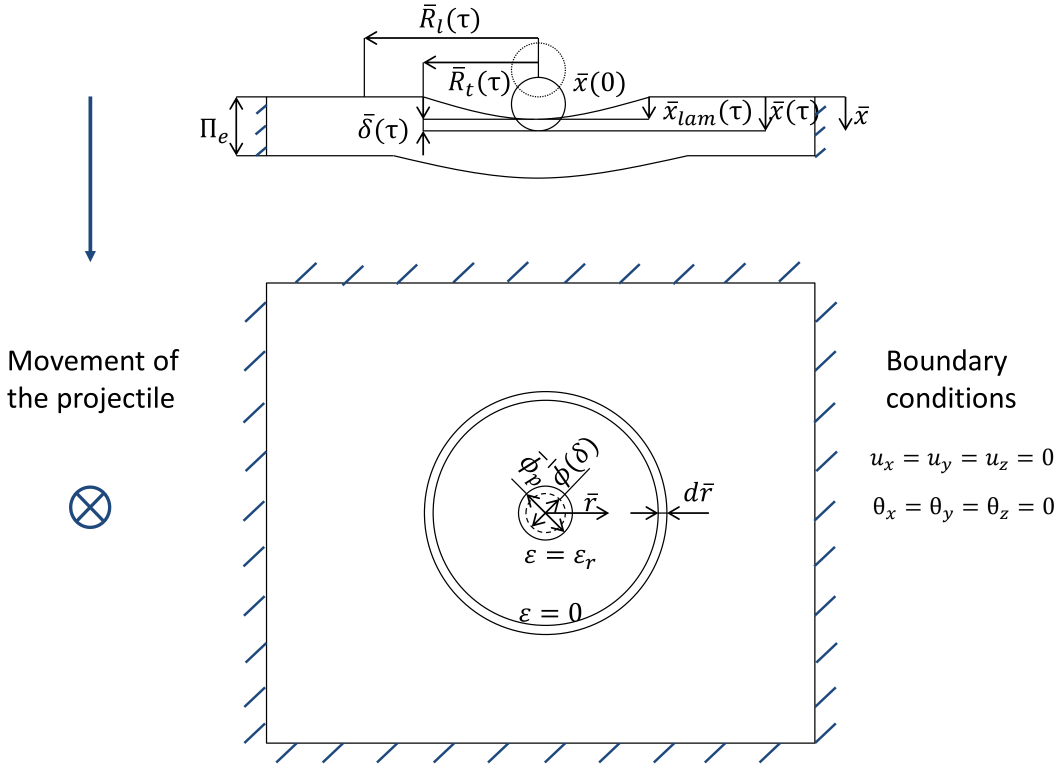

Figure 1: Schematic representation of a generic time instant of the impact process, showing the relevant variables.

Figure 1 shows a schematic representation of a generic instant of the impact process, where the variables and parameters described in the following sections can be easily identified. Note that an overbar designates a non-dimensional variable. The non-dimensional kinematic variables of the problem are: the projectile position $\bar{x}(\tau)$, the projectile velocity $\bar{v}(\tau)$ and the projectile acceleration $\bar{a}(\tau)$. The non-dimensional time τ is the integration variable.

2.1. Wave propagation and model

From the one dimensional wave theory (Smith et al., 1958), it can be stated that when a fibre is transversely impacted two waves are generated and propagate: (i) a longitudinal wave, C_l, which induces a steady tensile strain and travels at the elastic wave speed of the material, and (ii) a transverse wave, C_t, responsible for the acceleration of the laminate. These waves can be described as

$$C_l = \sqrt{\frac{\Pi_E}{\Pi_{\rho_l}}} \tag{4}$$

$$C_t = \sqrt{(1+\varepsilon_r)\frac{\Pi_{\sigma_r}}{\Pi_{\rho_l}}} - \sqrt{\frac{\Pi_E}{\Pi_{\rho_l}}}\varepsilon_r \tag{5}$$

where Π_E, Π_{σ_r}, ε_r and Π_{ρ_l} are the Π groups related to the Young's modulus, the in-plane failure stress, the in-plane failure strain and the laminate density, respectively. The transverse wave speed equation 5 is obtained as function of the steady strain for each particular impact velocity, considering fibres are linear-elastic before failure Smith et al. (1958). Inelastic waves may be also generated when a fibre is impacted. However, it seems a reasonable simplification to limit the analysis to the elastic waves, motivated on the almost perfectly linear-elastic response until failure of the in-plane mechanical behaviour of the laminate.

In Figure 1, the radii of the regions under longitudinal and transverse waves are, respectively,

$$\bar{R}_l(\tau) = C_l \tau \tag{6}$$

$$\bar{R}_t(\tau) = C_t \tau \tag{7}$$

Figure 2 shows the particle velocities at different locations on the laminate. Two different regions can be distinguished. The first one is dominated by the longitudinal wave, bounded between the longitudinal and transverse wave fronts (from point 2 to 3), while second region is dominated by the transverse wave, delimited by the transverse wave front (from point 1 to 2). Conventional models consider the longitudinal and transverse particle velocities of an impacted plate such as Moyre et al. (2000), Naik and Shrirao (2004), García-Castillo et al. (2009). The proposed model considers instead that the radial particle velocity, $\bar{v}_r(\tau)$, is constant between points 2 and 3, and decreases linearly to zero at the impact location (point 1). The particle transverse velocity, $\bar{v}_l(\tau)$, is assumed to be maximum at the impact (point 1), decreasing until reaching the transverse wave front, as shown in Figure 2.

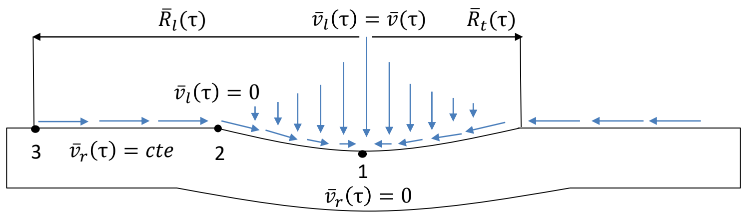

Figure 2: Schematic representation of the transverse and radial particle motion in the laminate.

With the progress of penetration through the laminate, the distance between the mid-plane of the plate and the centre of mass of the projectile decreases. The fibres fail through the thickness with the relative penetration of the projectile, neglecting potential out-of-plane mechanisms following the assumption of membrane behaviour. The penetration, $\bar{\delta}$, follows the relationship

$$\bar{\delta}(\tau, \bar{x}(\tau)) = \bar{x}(\tau) - \int_0^\tau \bar{v}_l(\tau) \mathrm{d}\tau \tag{8}$$

where $\bar{x}(\tau)$ is the location of the centre of mass of the projectile, and $\bar{v}_l(\tau)$ is an average velocity of the plate measured at the mid-plane. This velocity can be estimated by different approaches. When a high-velocity impact takes place and the transverse wave propagates, the movement of the laminate as a membrane is governed by a profile of velocities. In the contact point between the two bodies the velocity is the one of the projectile and a gradient is assumed up to the point reached by the transverse wave, where the transverse velocity is zero. Nevertheless, the accurate measurement of this profile with the experimental devices available nowadays is an impossible task. That is why we propose here a phenomenological function $\bar{k}(\tau, \bar{v}(\tau)) \in (0, 1]$, depending on the non-dimensional groups of the problem, instead of a profile of velocities. This function represents the percentage of the projectile velocity at which the laminate moves. Assuming this simplification, a constant velocity of the laminate as a whole can be estimated to calculate the penetration $\bar{\delta}$. This hypotheses will be checked with the FE model. Aiming at understanding the physically motivated ratios on which this phenomenological function depends, an explanation of the dimensional version of the function $k(t, v(t)) \in (0, 1]$ is given as

$$k(t, v(t)) = cD^{1/6} \left(\frac{v(t)}{v_i}\right)^2 \left(\frac{v_t t}{e}\right)^{1/2}, k \in (0, 1] \tag{9}$$

where D is the flexural rigidity of a plate defined in equation 10, c is a constant value of 0.25 $[\mathrm{N.m}]^{-1/6}$ and v_t is the transverse wave

$$D = \frac{Ee^3}{12(1-\nu^2)} \tag{10}$$

The function $k(t, v(t))$, can, therefore, be split into three parts. Attending to the flexural rigidity, the higher D, the higher $k(t, v(t))$. Therefore, the membrane behaviour will be more difficult to appreciate because the relative displacement will be very high and the laminate will have less time to bend. This behaviour can be observed in laminates where the stiffness is higher and, instead of a cone, a plug is formed (Cantwell and Morton, 1990; Kim et al., 2003; Rhymer et al., 2012). The relationship between $v(t)$ and V_i seems to be reasonable because at the beginning of the impact, when there is no damage, this ratio is higher leading to a $k(t, v(t))$ increase and the laminate moves almost like the projectile. Moreover, when the fibres and the matrix start to break, the relative displacement increases and also the difference between velocities, thus lowering this ratio. Finally, the ratio between the radius of the transverse wave and the thickness has a clear meaning because the lower this ratio (when the thickness increases), the lower the function $k(t, v(t))$ and it happens when the thickness increases. Therefore, $k(t, v(t))$ is lower, leading to higher difficulties to appreciate the projectile and the laminate moving together (membrane behaviour) when the thickness increases.

Rewriting $k(t, v(t))$ as a function of the Π groups of the problems leads to equation 11

$$\bar{k}(\tau, \bar{v}(\tau)) = \frac{\Pi_c}{\Pi_\nu} {\Pi_E}^{1/6} {C_{V_t}}^{1/2} \bar{v}(\tau)^2 \tau^{1/2}, \bar{k} \in (0, 1] \tag{11}$$

Finally, indentation during impact leads to a change of the contact surface between the projectile and the plate, resulting in an equivalent projected diameter

$$\bar{\phi}(\bar{\delta}) = \begin{cases} 2\sqrt{\bar{\delta} - \bar{\delta}^2}, & \text{if } \bar{\delta} < 0.5 \\ 1, & \text{if } \bar{\delta} \geq 0.5 \end{cases} \tag{12}$$

2.2. Energy absorption mechanisms

The general expression to calculate kinetic energy absorbed by the acceleration of the laminate, $\bar{E}_L$, assuming a certain profile of velocities can be described as

$$\bar{E}_L = \pi \Pi_e \Pi_{\rho_l} \int_0^{\bar{R}_t(\tau)} r \bar{v}(r, \tau)^2 \mathrm{d}\bar{r} \tag{13}$$

where the integral can be simplified by the equivalent laminate velocity at the mid-plane as it was explained in last section, leading to

$$\bar{E_L}(\tau) = \frac{1}{2} \pi \Pi_e \Pi_{\rho_l} \bar{R}_t(\tau)^2 \bar{v}_l(\tau)^2 \tag{14}$$

The second mechanism is the elastic energy absorbed by fibres, $\bar{E}_F$, corresponding to the area below the in-plane stress-strain curve, which can be calculated as

$$\bar{E}_F = \frac{1}{2} \Pi_E \varepsilon^2 \tag{15}$$

The contribution to this energy mechanisms can be divided in two different groups: (i) directly impacted, $\bar{E}_{TF}$, and (ii) adjacent fibres, $\bar{E}_{ED}$, (Moyre et al., 2000). Directly impacted fibres undergo tensile deformation due to the propagation of the longitudinal wave. Considering that the fibres break as the projectile goes through them, we can express a differential energy as a function of a differential relative displacement:

$$\mathrm{d}\bar{E}_{TF} = \Pi_B d\bar{\delta} \int_0^{\bar{R}_l(\tau)} \frac{1}{2} \Pi_E \varepsilon^2 \mathrm{d}\bar{r} \tag{16}$$

where Π_B is the Π group related to the yarn width. The strain gradient along the yarn direction can be defined by the following expression, proposed by Naik et al. (2006):

$$\varepsilon = \varepsilon_r b^{\frac{\bar{r}}{\Pi_B}} \tag{17}$$

where $\bar{r}$, b and ε_r are the radial coordinate, the stress wave transmission factor and the in-plane failure strain, respectively. The strain is maximum at the impact point, and decays radially. If maximum strain is at the impact point, failure breakage is initiated at the impact point.

The volume of fibres involved in tensile failure, $\bar{V}_{TF}$, is driven by the penetration of the projectile and the circular area given by the radius of the longitudinal wave. The projectile is assumed to be big enough to impact on two perpendicular yarns directly with an inherent volume:

$$\bar{V}_{TF}(\tau) = 4\Pi_B \bar{\delta}(\tau)\bar{R}_l(\tau) \tag{18}$$

Therefore, the final elastic energy absorbed by fibre failure can be obtained considering the symmetry of the cross-ply laminate. Dividing equation 16 with respect to non-dimensional time and rearranging terms, provides:

$$\bar{E}_{TF}(\tau) = \frac{\Pi_B \Pi_E \varepsilon_r^2}{\ln(b)} \int_0^{\tau} \bar{v}(\tau)\left\{1 - \bar{k}\left[\tau, \bar{v}(\tau)\right]\right\}\left(b^{\frac{2C_l\tau}{\Pi_B}} - 1\right) \mathrm{d}\tau \tag{19}$$

Adjacent fibres, bounded by the contact area of the projectile $\bar{\phi}(\bar{\delta})$ and the transverse wave front, will be under linear elastic deformation defined by a linear gradient, which assumes maximum strains are reached at the periphery of the projectile and zero at the transverse wave front, that is,

$$\varepsilon = \varepsilon_r \left[\frac{2(\bar{R}_t(\tau) - \bar{r})}{2\bar{R}_t(\tau) - \bar{\phi}(\bar{\delta})}\right] \tag{20}$$

with an associated volume, $\bar{V}_{ED}$, given by:

$$\bar{V}_{ED}(\tau) = \pi\Pi_e \left(\bar{R}_t(\tau)^2 - \frac{\bar{\phi}(\bar{\delta})^2}{4}\right) \tag{21}$$

resulting in the final expression:

$$\bar{E}_{ED}(\tau) = \pi\Pi_e\Pi_E \int_{\frac{\bar{\phi}(\bar{\delta})}{2}}^{\bar{R}_t(\tau)} \varepsilon^2 \bar{r}\mathrm{d}\bar{r} \tag{22}$$

Additional energy absorption mechanisms have been identified as matrix cracking, $\bar{E}_{MC}$, and delamination, $\bar{E}_{DL}$. Matrix failure is controlled by the transverse wave and bending of the laminate, resulting in a circular shaped damaged area (Alonso et al., 2018b; Gil-Alba et al., 2019). Total energies absorbed by matrix cracking and delamination are defined, respectively as

$$\bar{E}_{MC}(\tau) = \pi\alpha_{MC}\Pi_e\Pi_{E_{MT}}\bar{R}_t(\tau)^2 \tag{23}$$

$$\bar{E}_{DL}(\tau) = \pi\alpha_{DL}\Pi_{G_{IICD}}\bar{R}_t(\tau)^2 \tag{24}$$

2.3. Energy balance

The model is formulated by means of an energy balance. This balance may be written in its dimensional form as

$$E_0 = E_p(t) + E_{AB}(t) \tag{25}$$

This instantaneous balance is valid for any time t and implies that the initial kinetic energy of the projectile, E_0, is equal to the sum of the kinetic energy of the projectile at any time instant, $E_p(t)$, to the energy absorbed by all the mechanisms described above at that same time, $E_{AB}(t)$. In the non-dimensional formulation, this balance becomes

$$1 = \bar{v}(\tau)^2 + \frac{12}{\pi}\bar{E}_{AB}(\tau) \tag{26}$$

where $\bar{E}_{AB}(\tau)$ is

$$\bar{E}_{AB}(\tau) = \bar{E}_L(\tau) + \bar{E}_{ED}(\tau) + \bar{E}_{TF}(\tau) + \bar{E}_{DL}(\tau) + \bar{E}_{MC}(\tau) \tag{27}$$

The balance of Eq. (27) is derived with respect to the non-dimensional time providing the expression of Eq. (28) with its corresponding initial conditions:

$$\begin{gathered}
\bar{a}(\tau) = \frac{\bar{g}(\tau,\bar{x}(\tau),\bar{v}(\tau)) - \bar{h}(\tau,\bar{v}(\tau))\bar{v}(\tau)}{\frac{\pi}{6}\bar{v}(\tau) + \pi\Pi_e\Pi_{\rho_l}{C_{V_t}}^2[2\tau^{5/2}\bar{k}(\tau,\bar{v}(\tau))\frac{\Pi_c}{\Pi_\nu}{\Pi_E}^{1/6}{C_{V_t}}^{1/2}\bar{v}(\tau)^3 + \tau^2\bar{k}(\tau,\bar{v}(\tau))^2\bar{v}(\tau)]} - \\
- \frac{\pi\Pi_e\Pi_{\rho_l}{C_{V_t}}^2[\tau\bar{k}(\tau,\bar{v}(\tau))^2\bar{v}(\tau)^2 + \tau^{3/2}\bar{k}(\tau,\bar{v}(\tau))\frac{\Pi_c}{2\Pi_\nu}{\Pi_E}^{1/6}{C_{V_t}}^{1/2}\bar{v}(\tau)^4]}{\frac{\pi}{6}\bar{v}(\tau) + \pi\Pi_e\Pi_{\rho_l}{C_{V_t}}^2[2\tau^{5/2}\bar{k}(\tau,\bar{v}(\tau))\frac{\Pi_c}{\Pi_\nu}{\Pi_E}^{1/6}{C_{V_t}}^{1/2}\bar{v}(\tau)^3 + \tau^2\bar{k}(\tau,\bar{v}(\tau))^2\bar{v}(\tau)]} \\
\bar{x}(0) = 0 \\
\bar{v}(0) = 1
\end{gathered} \tag{28}$$

The stop condition of the model is:

$$\bar{\delta}(\tau) = \Pi_e \tag{29}$$

Functions (30) and (31) are defined to facilitate the handling of equations:

$$\bar{h}(\tau,\bar{v}(\tau)) = \frac{d\bar{E}_{TF}(\tau)}{d\tau}\frac{1}{\bar{v}(\tau)} \tag{30}$$

$$\bar{g}(\tau,\bar{x}(\tau),\bar{v}(\tau)) = \begin{cases} -\frac{d}{d\tau}[\bar{E}_{DL}(\tau) + \bar{E}_{MC}(\tau)], & \text{if } \tau \leq \frac{\bar{\phi}(\bar{\delta})}{2C_{V_t}} \\ -\frac{d}{d\tau}[\bar{E}_{ED}(\tau) + \bar{E}_{DL}(\tau) + \bar{E}_{MC}(\tau)], & \text{if } \tau > \frac{\bar{\phi}(\bar{\delta})}{2C_{V_t}} \end{cases} \tag{31}$$

This second-order non-linear differential equation can be solved by numerical integration. Integrating this equation, the velocity and the position of the projectile can be obtained. Furthermore, once the problem is solved, by substituting the outputs in Eq. (28), the acceleration of the projectile is obtained and thus all the kinematic variables of the problem.

3. Numerical modelling

To fully validate the theoretical model presented in the previous section, a 3D numerical model previously developed by the authors has been additionally used (Alonso et al., 2020), where all the properties needed for this model can be found. This model is based on a continuum damage mechanics approach and defines the failure criteria with equivalences to the ones contemplated by the theoretical model (Hashin, 1980; Muñoz et al., 2015; Chang and Chang, 1987; Menna et al., 2011). The constitutive response of the material is linear-elastic up to the onset of damage and can be described in Mandel's notation as

$$\begin{bmatrix} \varepsilon_{11} \\ \varepsilon_{22} \\ \varepsilon_{33} \\ \gamma_{12} \\ \gamma_{23} \\ \gamma_{13} \end{bmatrix} = \begin{bmatrix} \frac{1}{E_{11}(1-d_1)} & -\frac{\nu_{21}}{E_{22}} & -\frac{\nu_{31}}{E_{33}} & 0 & 0 & 0 \\ -\frac{\nu_{12}}{E_{11}} & \frac{1}{E_{22}(1-d_2)} & -\frac{\nu_{32}}{E_{33}} & 0 & 0 & 0 \\ -\frac{\nu_{13}}{E_{11}} & -\frac{\nu_{23}}{E_{22}} & \frac{1}{E_{33}(1-d_3)} & 0 & 0 & 0 \\ 0 & 0 & 0 & \frac{1}{G_{12}(1-d_4)} & 0 & 0 \\ 0 & 0 & 0 & 0 & \frac{1}{G_{23}(1-d_5)} & 0 \\ 0 & 0 & 0 & 0 & 0 & \frac{1}{G_{13}(1-d_6)} \end{bmatrix} \begin{bmatrix} \sigma_{11} \\ \sigma_{22} \\ \sigma_{33} \\ \sigma_{12} \\ \sigma_{23} \\ \sigma_{13} \end{bmatrix} \tag{32}$$

where ε_{ii} and γ_{ij} (with $i = 1, 2, 3$ and $j = 1, 2, 3$) are the components of the strain tensor, σ_{ij} are the components of the stress tensor; E_{ij}, ν_{ij} and G_{ij} are the Young's moduli, Poisson's ratios and shear moduli, respectively, and d_i are damage parameters associated to different failure mechanisms. The evolution of the damage variables is controlled by the fracture toughness along each direction, leading to a linear decay once the onset of damage has been reached.

3.1. Failure modelling

Failure mechanisms can be either in-plane and out-of-plane. The theoretical model for thin laminates presented in Section 2 accounts for in-plane energy absorption mechanisms such as fibre breakage and matrix failure, and neglects the contribution of shear plugging and crushing. The proposed 3D numerical model, however, includes all the energy absorption mechanisms involved in ballistics to further validate the applicability range of the theoretical model (Alonso et al., 2018a, 2020).

In-plane tensile and compression fibre failure are triggered once the following criteria are reached Chang and Chang (1987):

$$\left(\frac{\sigma_{11}}{X_{11i}}\right)^2 + \left(\frac{\sigma_{12}}{S_{12}}\right)^2 + \left(\frac{\sigma_{13}}{S_{13}}\right)^2 = 1 \tag{33}$$

$$\left(\frac{\sigma_{22}}{X_{22i}}\right)^2 + \left(\frac{\sigma_{12}}{S_{12}}\right)^2 + \left(\frac{\sigma_{13}}{S_{13}}\right)^2 = 1 \tag{34}$$

where X_{lkr} and S_{lk} are the normal and shear failure stresses respectively associated to $l = 1, 2, 3$ and $k = 1, 2, 3$. $r = (t, c)$ accounts for tension and compression.

Failure by matrix cracking is assumed to be caused by in-plane shear tension according to Hashin (1980), leading to

$$\left(\frac{\sigma_{12}}{S_{12s}}\right)^2 = 1 \tag{35}$$

where S_{12s} is the maximum shear strength (Xiao et al., 2007). The through-thickness matrix and fibre failure criterion is associated to shear plugging and the onset of failure is given by

$$\left(\frac{\sigma_{13}}{S_{13s}}\right)^2 + \left(\frac{\sigma_{23}}{S_{23s}}\right)^2 = 1 \tag{36}$$

The crush failure criterion is associated to compression along the thickness of the laminate, as described by

$$\left(\frac{\sigma_{33}}{X_{33}}\right)^2 = 1 \tag{37}$$

Finally, the interlaminar damage model used in the finite element analyses is based on the classical cohesive zone method by means of a traction-separation law (Turon et al., 2007). Damaged is assumed to initiate when the following criterion is met,

$$\left(\frac{\langle t_n \rangle}{N}\right)^2 + \left(\frac{t_s}{S}\right)^2 + \left(\frac{t_t}{S}\right)^2 = 1 \tag{38}$$

where t_n, t_s and t_t are the normal and shear stresses, respectively, and N, S are the damage threshold normal and shear strengths of the cohesive elements. The Benzeggagh-Kenane (BK) fracture criterion (Kenane and Benzeggagh, 1997) governs the evolution of damage after the onset of failure,

$$\Gamma^C = {\Gamma_n}^C + ({\Gamma_s}^C - {\Gamma_n}^C)\left(\frac{\Gamma_s + \Gamma_t}{\Gamma_n + \Gamma_s + \Gamma_t}\right)^\eta \tag{39}$$

where ${\Gamma_n}^C$ and ${\Gamma_s}^C$ are defined as the critical energy release rates for delamination in modes I and II, which correspond to pure tension and shear mode, respectively. Γ_n, Γ_s and Γ_t account for the work dissipated due to the displacements along the normal and shear directions, caused by normal and shear stresses, respectively. η is a characteristic parameter of the BK law that accounts for the increase in toughness with the mode mixity (Abaqus6.14, 2014).

Further details about the failure modelling can be found in Alonso et al. (2020).

3.2. FE Implementation

The finite element simulations were carried out using Lagrangian 3D elements. The dimensions of the plates were the same than the experimental tests (150x150 [mm^2]). To simulate the plates, reduced integration solid elements were used (Abaqus C3D8R). Cohesive elements were used to simulate the joint between the plies (Abaqus COH3D8). A convergence study was carried out to ensure the validity of the results. The mesh was divided in two regions, the impact zone and its surroundings, where the density of elements is higher leading to a finer mesh, and the rest, where the density of elements decay gradually as long as the region is further away from the impact zone resulting into a coarser mesh. A number of 10 and 20 solid elements were used along the thickness direction for 3 mm and 6 mm thick specimens, respectively. For the cohesive elements, 1 element (0.001 mm thick) was used along the thickness direction to simulate the joint between two plies. The projectile (density 7800 kg.m^{-3} and diameter 7.5 mm) was simulated as a spherical analytical surface and an exponential decay friction model was used to simulate the friction between projectile and target. Regarding the boundary conditions, the projectile was constrained to only move though the thickness direction and the exterior borders of the laminate were clamped. The elements were removed when any of the damage variables reached the value of 1. Further details of the finite element model implementation can be found in Alonso et al. (2020).

4. Results and discussion

This section describes the results obtained with the theoretical model and compares these with the finite element analysis. The theoretical model is first validated with residual velocities obtained experimentally. Secondly, both models are used to analyse the influence of geometrical characteristics and material properties on the protective capability of thin woven laminates against ballistic impacts.

4.1. Validation of the theoretical model

The theoretical model is validated with experimental results from the ballistic response of E-glass/Polyester woven laminates of 3 and 6 mm thickness (Buitrago-Pérez et al., 2010). The laminates tested were clamped in a steel frame. Then, a 7.5 mm steel projectile was propelled against the laminate. Helium was used in a pressurised chamber to propel the impactor.

A comparison between the predicted theoretical, numerical and experimental residual velocities is shown in Figure 3. The theoretical ballistic limit is the impact velocity at which the residual velocity is different from zero. Note that for the determination of the experimental and numerical ballistic limit, the Lambert-Jonas equation was used to adjust the experimental and numerical data curves (Lambert and Jonas, 1976),

$$v_r = A\left(v_i^p - v_{bl}^p\right)^{\frac{1}{p}} \tag{40}$$

where A and p are empirical parameters.

Good agreement with the theoretical model is observed for both the ballistic limit and the absorbed energy. The thinner laminate performs better, with the highest error (10%) obtained for the ballistic limit of the 6 mm thickness plate. The inversion of the curves for the thicker laminates (Figure 3) can be explained as follows. This model is based on the assumption that the laminate behaves as a membrane, bending and accelerating, and this assumption is proven to work very well for 3 mm. Nevertheless, 6 mm is very close to the threshold found by (Alonso et al., 2018a) from which a laminate can be considered thick. Consequently, since this model, as Figure 9 shows, gives an essential importance to energy-absorption mechanisms such as elastic deformation of fibres (a part of FF) or acceleration of the laminate (A), which are in fact higher in the ballistic limit because the contact time is maximum, it does not reproduce so accurately the behaviour for 6 mm thick panels because the bending and elastic deformation of fibres is more difficult to appreciate when the thickness increases. Therefore, since bending and thus acceleration of the laminate and elastic deformation of fibres absorb less energy, the model overestimates the energy absorbed and so the ballistic limit.

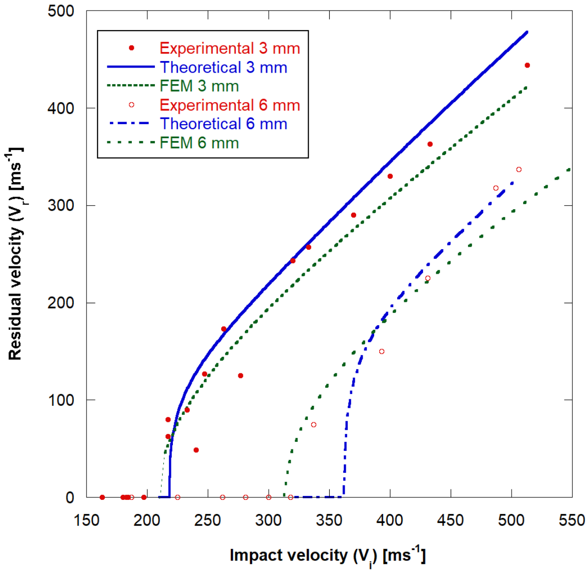

Figure 3: Comparison of experimental Buitrago-Pérez et al. (2010) and numerical results with the proposed theoretical model.

To fully validate the theoretical model it is necessary to check if the simplification of the wave theory on which the model is based is reasonable. We considered that the laminate is homogeneous and thus we used a longitudinal wave velocity with the homogenized properties of the laminate. To validate this hypothesis, the propagation of the longitudinal wave was measured in the FE model and compared to the simplified theoretical prediction. Two cases near the ballistic limit were analysed; 3 mm and 6 mm thickness plates impacted at velocities of 240 $m.s^{-1}$ and 337 $m.s^{-1}$ respectively. The theoretical longitudinal radius prediction was calculated as the longitudinal wave velocity times the time while the FEM prediction was calculated analysing the integration point of an element at a desired instant. By the time the stress is different from zero in the integration point, the longitudinal wave was considered to reach the element. Figure 4 shows the comparison between the theoretical and FE predictions of the longitudinal wave radii for the two cases analysed. An almost perfect agreement is observed between theoretical and FE predictions for both cases. It means that the assumption related to the longitudinal wave velocity in the theoretical model is valid.

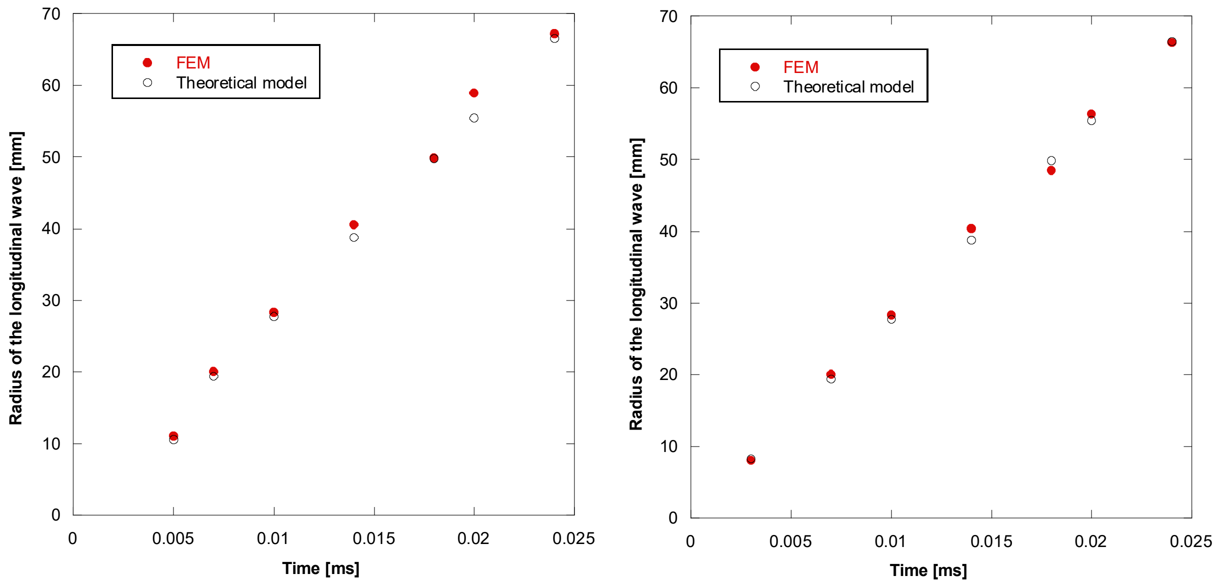

(a) *(b)*

Figure 4: Comparison of the theoretical and numerical predictions of the longitudinal wave radii for (a) a 3 *mm thick laminate subjected to an impact velocity of* 240m.s^{-1} *(b) a* 6 *mm thick laminate subjected to an impact velocity of* 337m.s^{-1}.

4.2. Analysis of the Π *groups of the problem*

The performance of the proposed theoretical model is assessed through a number of analysis of the Π groups of the problem, the influence of the laminate thickness and projectile diameter on the ballistic limit. The corresponding results are shown in Figure 5a for thickness-to-diameter ratios (Π_e) of 0.85, 1 and 1.15. As expected, the predicted ballistic limit increases with the ratio Π_e. The three cases analysed present the same behaviour. Figure 5a shows that the ballistic limit decreases when increasing the projectile diameter even though the thickness increases in the same magnitude since Π_e remains constant. Eventually the ballistic limit tends to an asymptote in the range analysed for thin laminates. To explain these results, Figure 5b shows the projectile mass grows faster than the laminate mass. As a consequence, the projectile penetrates easier into the laminate due to the fast growth of the impactor kinetic energy. The shape of the curves showed in Figure 5 is the same suggesting that the ballistic limit is governed by the mass laminate-mass projectile ratio.

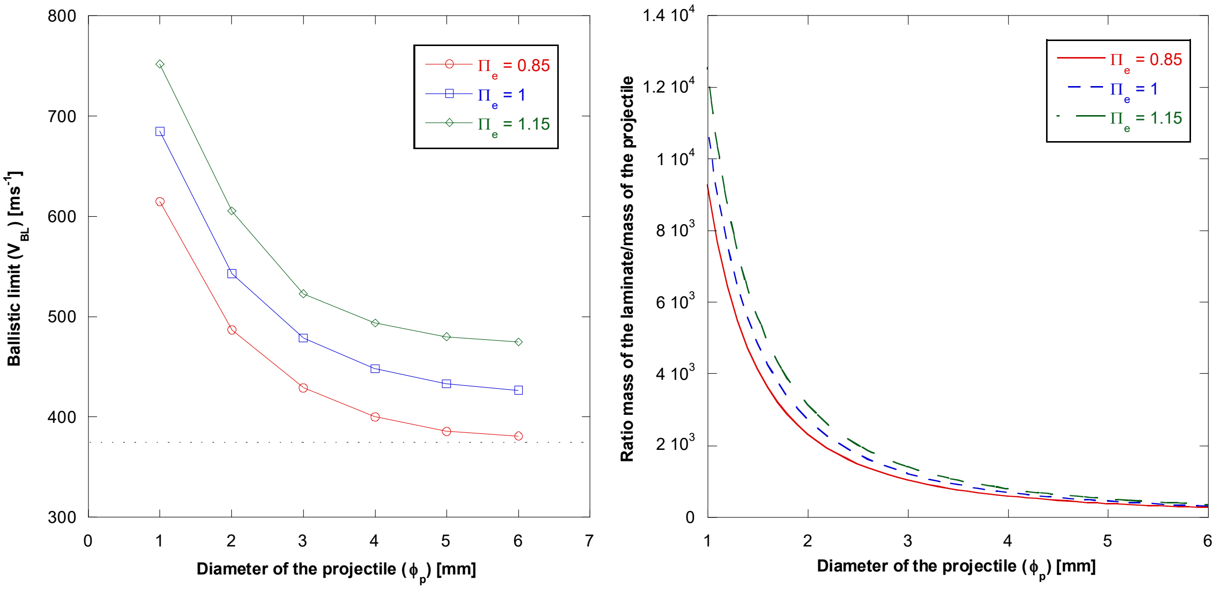

(a) *(b)*

Figure 5: (a) Theoretical model ballistic limit predictions for different thickness-to-diameter ratios ($\Pi_e = 0.85$*,* $\Pi_e = 1$ *and* $\Pi_e = 1.15$*) (b) Mass of the laminate / mass of the projectile ratios for different thickness-to-diameter ratios (*$\Pi_e = 0.85$*,* $\Pi_e = 1$ *and* $\Pi_e = 1.15$*).*

The results in Figure 6 show the influence of the Young's modulus in direction 11 (E_{11}) on the ballistic limit of the laminate, for thicknesses of 3 and 6 mm. The ballistic limit increases with the E_{11}, with this effect becoming more evident for the higher thickness laminate. Thicker laminates absorb more energy and thus the ballistic curves of Figure 6b are shifted to the the right compared to Figure 6b. The ballistic limit grows with E_{11} because the energy absorbed by elastic deformation and tensile failure of fibres, which are the most important energy-absorption mechanisms near the ballistic limit, increases following Eqs. (22), (19) show. Therefore, the results in terms of the ballistic limit are physically consistent since the laminate capability to stop the projectile is expected to be greater if the in-plane stiffness grows. Moreover, all the curves collapse into one for higher velocities. This result can be explained by the fact that, if the impact velocity tends to infinite, the absorption capability of the laminate tends to zero regardless of the material properties.

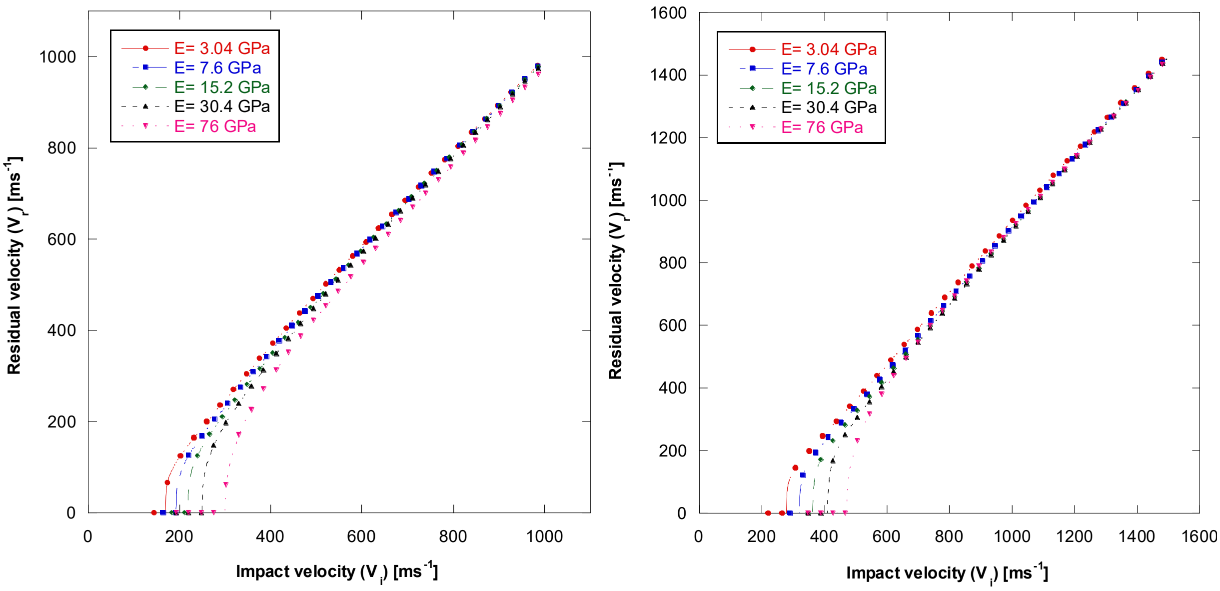

(a) *(b)*

Figure 6: Residual velocity curves for the (a) 3 *mm and (b)* 6 *mm laminates: Influence of the Young's modulus in direction 11 in the energy absorption capacity of the laminate.*

4.3. Plate penetration

Penetration is evaluated for laminates with 3 and 6 mm thickness, and three ballistic regimes, below the ballistic limit, where no complete penetration occurs (197 and 262 m.s^{-1} respectively), at the ballistic limit (240 and 337 m.s^{-1} respectively) and above the ballistic limit (320 and 487 m.s^{-1} respectively).

The theoretical prediction of the penetration rate $\bar{\delta}$ is validated with numerical simulations. This is a way to validate the hypothesis of the relative displacement formulated in the theoretical model by means of the phenomenological function $\bar{k}(\tau, \bar{v}(\tau))$. In the numerical model, the penetration is calculated as the relative displacement between the centre of mass of the projectile, $x(t)$, and the rear face of the laminate, $x_l(t)$. Figure 7 illustrates an instant of time from where the projectile does not interact anymore with the laminate for a full penetration case in a FE simulation.

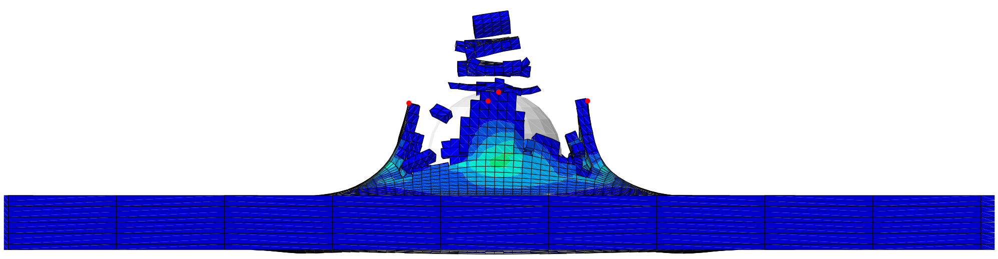

Figure 7: Instant of time in one of the numerical simulations from where the projectile does not interact anymore with the laminate.

The observed correlation between numerical and theoretical penetration values is shown in Figure 8 for the laminates with 3 and 6 mm thickness, respectively. Simulations have been conducted at velocities below (Figures 8a, 8d), near (Figures 8b, 8e) and above (Figures 8c, 8f) the ballistic limit. Good agreement between theoretical and numerical results is observed for both panels at velocities below the ballistic limit

(Figures 8a, 8d). Final penetration predicted by both models matches as shown in Figures 8a, 8d.A good enough agreement is observed for ballistic limit velocities for the laminate with 3 mm thickness (Figure 8b). However, for laminates with 6 mm thickness (Figure 8e), the numerical model overestimates the relative displacement between both bodies compared to the theoretical model. The differences are caused because full penetration occurs in the FE model while the projectile gets stuck in the theoretical model (note that the relative displacement does not reach the value of 1 in the theoretical model prediction). Last, Figures 8c, 8f show a similar prediction of both models for plates subjected to impact velocities above the ballistic limit. Nevertheless, the predictions are more similar for the 3 mm thickness case. Overall, the worse agreement for thicker laminates can be explained by the study carried out by Alonso et al., 2018. The hypothesis of membrane behaviour assumed in this theoretical model works worse with thickness increase, with 6 mm being very close to the transition from thin to thick laminate. Therefore, the prediction of parameters related to this hypothesis is expected to worsen with thickness increase, as shown in Figure 8. In addition, other effects assumed negligible in the theoretical model such as through-thickness failure mechanisms become more important and are not properly captured.

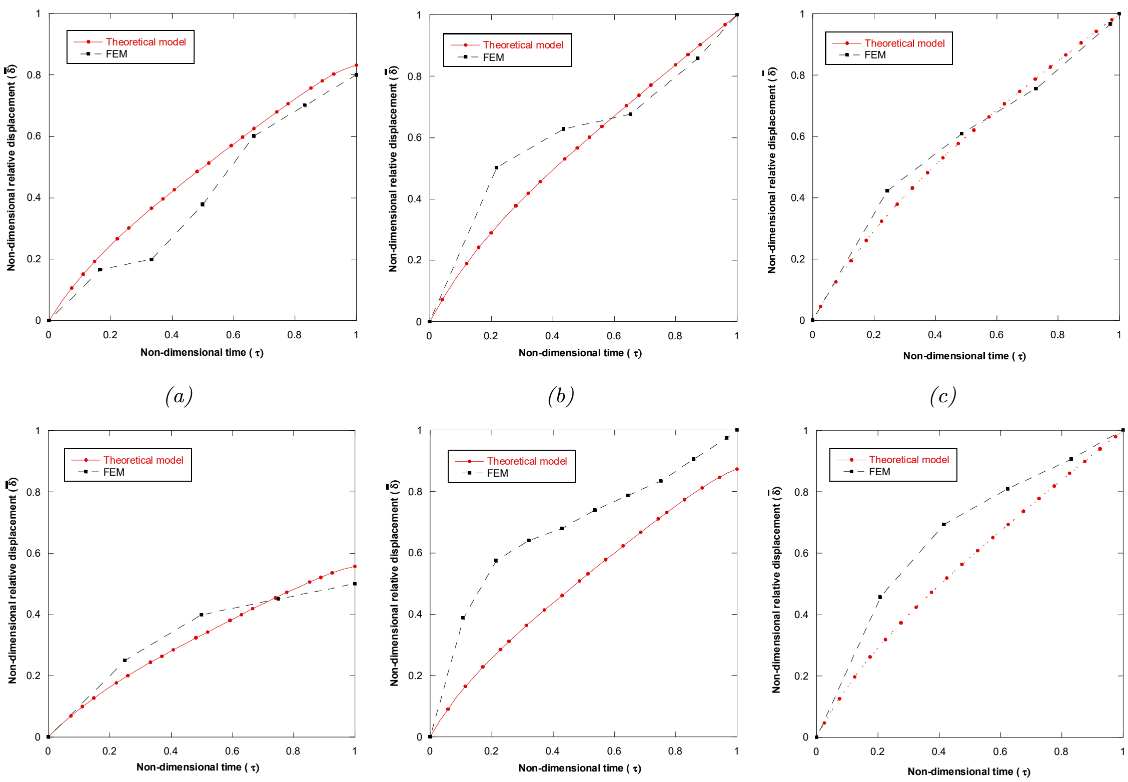

(a) *(b)* *(c)*

(d) *(e)* *(f)*

Figure 8: Penetration, $\bar{\delta}$, vs non-dimensional time for 3 mm laminates, for impact velocities of (a) 197m.s^{-1}*, (b)* 240m.s^{-1} *and (c)* 320m.s^{-1} *and for 6 mm laminates, for impact velocities of (d)* 262m.s^{-1}*, (e)* 337m.s^{-1} *and (f)* 487m.s^{-1}.

4.4. Failure mechanisms and energy absorption

A comparison between the numerical and theoretical model predictions of the energy absorbed by each individual mechanism is presented in the following paragraphs. The following mechanisms are accounted for in the theoretical model: (i) fibre failure (see equations 33 and 34) is associated to elastic deformation and tensile failure of fibres; (ii) matrix failure (see equation 37) is associated with matrix cracking; (iii) kinetic energy of the elements is associated to kinetic energy of the laminate. Crush failure and shear driven failure (see equations 35 and 36) are not contemplated in the theoretical model. We assume this hypothesis since it has been demonstrated that these mechanisms do not play a major role in the penetration process for thin laminates (Alonso et al., 2020). Note that friction is another energy dissipation process present during the whole impact process but it is considered negligible under the thin laminates hypotheses and thus it is not shown in Figure 9 in the FEM part. The numerical energy results are determined using the methodology proposed by (Alonso et al., 2020).

The comparison of the absorbed energy fractions of each mechanism is shown in Figure 9 for the 3 and 6 mm laminates, respectively. This study has been carried out at the same velocities as the penetration analysis. The main energy-absorption mechanisms observed in this analysis is fibre breakage (corresponding to elastic deformation and tensile failure of fibres in the theoretical model), being even more important below the ballistic limit. Matrix cracking and delamination are proved to have a minor role in all the cases analysed despite the ballistic regime. Nevertheless, the remaining energy is dissipated mostly by through-thickness failure mechanisms, such as crushing and shear plugging, with higher influence of crushing for velocities above the ballistic limit. The influence of this mechanism is higher for 6 mm laminates since the laminate is closed to be considered as thick Alonso et al. (2018a). At higher velocities, the fibre breakage occurs fast and thus the energy absorbed by this mechanism is less important. Therefore, the shear and through-thickness resistances gain importance as shown in Figures 9c, 9f. Consequently, fibre failure and compression are the most important energy-absorption mechanisms for 6 mm laminates. The kinetic energy absorbed by the laminate acceleration increases its importance when full penetration occurs since the laminate keeps moving at the moment of complete penetration as Figures 9c, 9f show. Note that the energy absorbed by the laminate acceleration is recoverable.

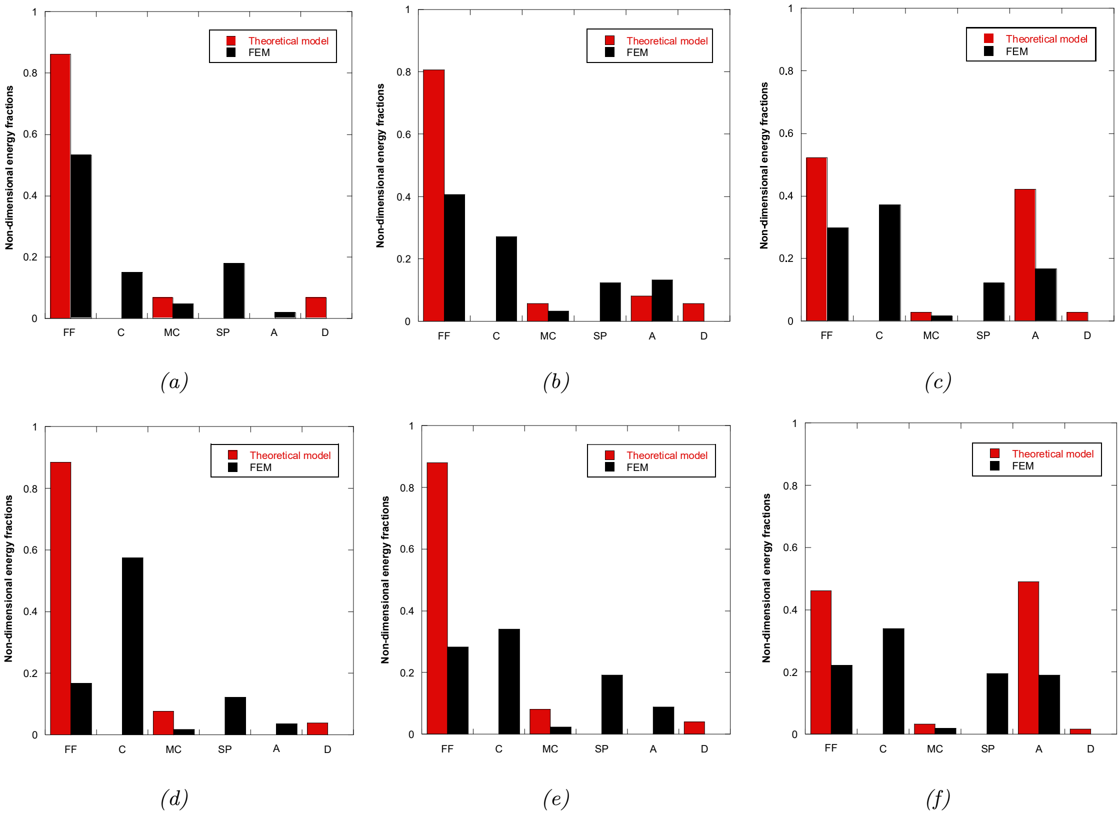

Figure 9: Theoretical and numerical non-dimensional energy fractions from left to right: Fibre failure (FF), compression (C), matrix cracking (MC), shear plugging (SP), acceleration of the laminate (A) and delamination (D) for a 3 *mm thick specimen subjected to velocities of (a)* 197m.s^{-1}, *(b)* 240m.s^{-1} *and (c)* 320m.s^{-1} *and for a* 6 *mm thick specimen subjected to velocities of (d)* 262m.s^{-1}, *(e)* 337m.s^{-1} *and (f)* 487m.s^{-1}.

Overall, both theoretical and FE predictions are consistent in terms of the relative roles of energy-absorption mechanisms. Note that the FE model accounts for a wide variety of energy absorption mechanisms. Despite this fact, the main trends observed in both theoretical and FE approaches are consistent.

4.5. Comparison with flat-ended projectile

The versatility of the theoretical model allows for a change in the impactor shape. The impact behaviour of 3 mm and 6 mm thick specimens subjected to flat-ended projectile impacts with the same diameter and mass (7.5 mm and 1.725 g) is studied. Since there are not experimental data available, the main objective of this section is to compare the influence of the projectile shape in the theoretical model predictions. To carry out this study, the projected area of the projectile has to be changed, therefore equation 12 becomes in equation 41 and all the equations in which $\bar{\phi}(\bar{\delta})$ is involved change accordingly,

$$\bar{\phi}(\bar{\delta}) = \frac{\phi_p}{e} \tag{41}$$

Figure 10 shows a comparison between the predicted theoretical residual velocities for the two thicknesses and projectile shapes analysed.

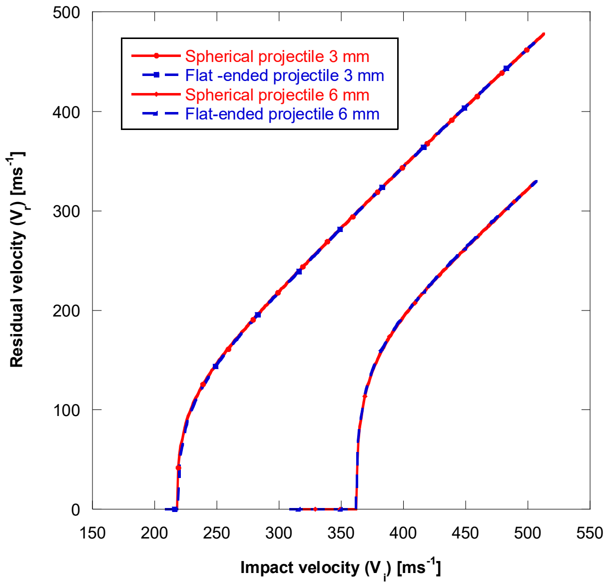

Figure 10: Comparison between the predicted theoretical ballistic response for 3 *mm and* 6 *mm laminates impacted by spherical and flat-ended projectiles.*

Good agreement between the two shapes is observed. Actually, the curves almost overlap. From this, it can be inferred that the projectile shape has not an important influence on the ballistic response as long as the diameter and mass remain constant, which is in agreement with previous works (Ulven et al., 2003).

Another important point to check is if the hypotheses for thin laminates are met when changing the projectile shape. To accomplish that, the predicted theoretical and numerical relative displacement versus time for velocities below the ballistic limit are shown in Figure 11 for the two thicknesses.

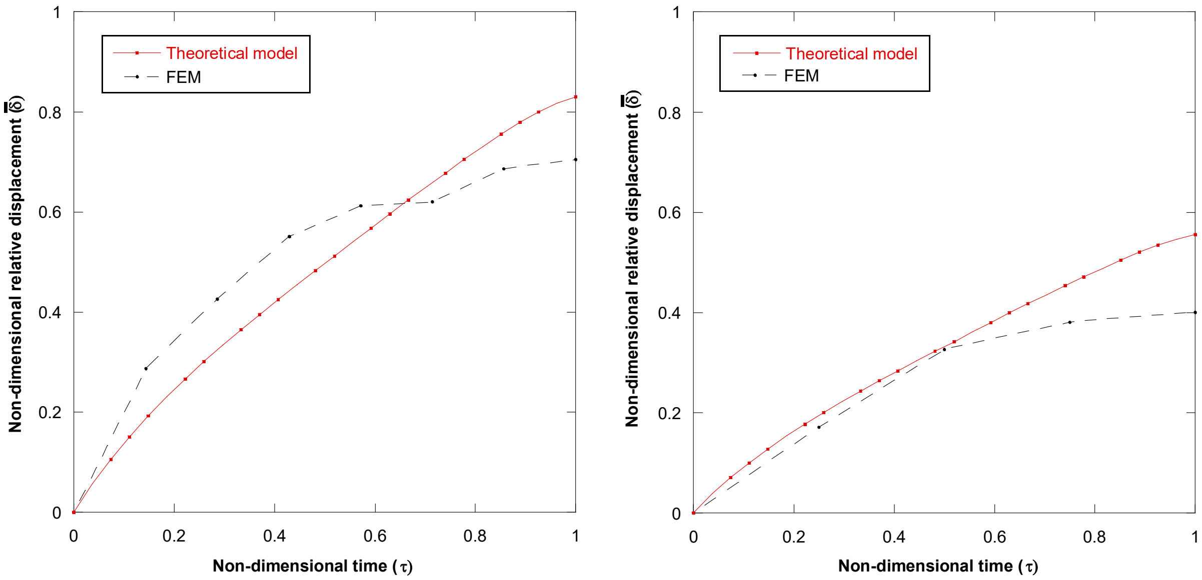

(a) *(b)*

Figure 11: Flat-ended projectile penetration, $\bar{\delta}$, vs non-dimensional time for 3 *mm laminates, for an impact velocity of (a)* $197 \mathrm{m.s}^{-1}$*, and for* 6 *mm laminates, for an impact velocity of (b)* $262 \mathrm{m.s}^{-1}$.

Figure 11 shows a good agreement between theoretical and numerical results for both thicknesses. Nevertheless, the difference in the predicted final penetration observed in Figure 11b is higher than in Figure 11a. Again, this is a consequence of the laminate thickness since the higher the thickness, the worse the suitability of the thin laminate hypotheses considered.

Figure 12 shows a comparison between the two models' prediction by means of the relative importance of the energy-absorption mechanisms for the same two velocities.

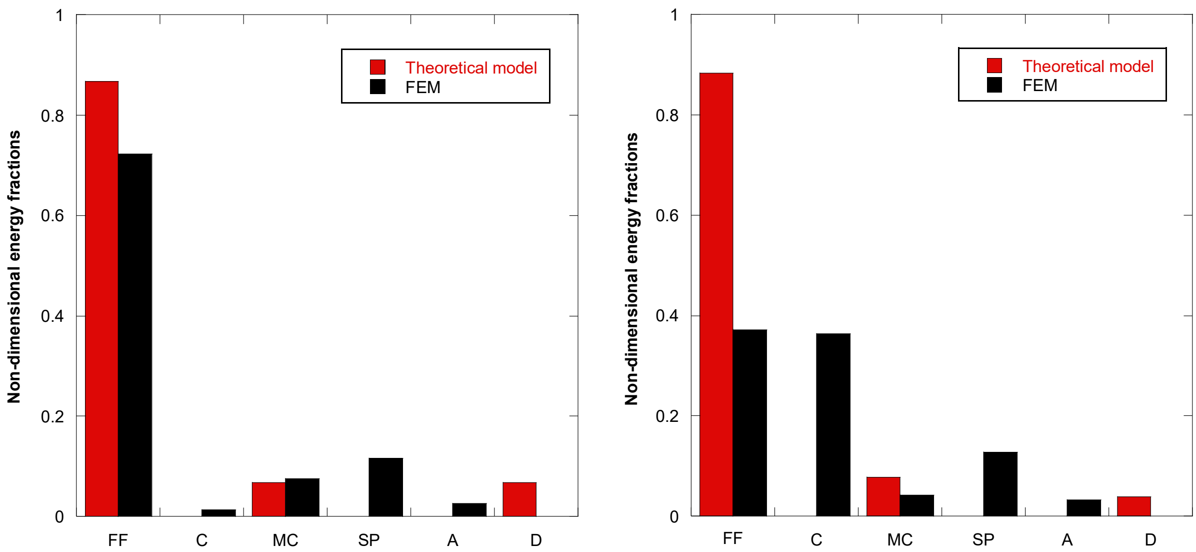

(a) *(b)*

Figure 12: Theoretical and numerical non-dimensional energy fractions from left to right: Fibre failure (FF), compression (C), matrix cracking (MC), shear plugging (SP), acceleration of the laminate (A) and delamination (D) for a specimen impacted by a flat-ended projectile with an impact velocity of (a) $197 \mathrm{m.s}^{-1}$ *for* 3 *mm thickness and (b)* $262 \mathrm{m.s}^{-1}$ *for* 6 *mm thickness.*

Overall, the relative importance of the terms is the same than predicted in Figures 9a, 9d. Fibre failure is the most important energy-absorption mechanism and out-of-plane energy-absorption mechanisms increase with thickness. Nevertheless, in Figure 12b fibre failure and compression share the dominant role while in Figure 9d compression is significantly more important. It makes sense that fibre failure is more important for flat-ended projectiles since the whole diameter is in contact from the beginning contributing to fibre breakage. Therefore, it can be inferred that, although the ballistic response is almost the same, the relative contribution of the energy-absorption mechanisms/failure modes can change with the projectile shape.

5. Conclusions

The ballistic impact of thin woven E-glass fibre/polyester composites was studied in this paper, and a new theoretical model was proposed to describe the mechanical response and penetration of the laminates. The non-dimensional energy-based theoretical model considers traditional energy absorption mechanisms from previous models, and incorporates new hypotheses. The main governing equation of the problem is a non-linear second-order differential equation on the position of the projectile with respect to the laminate front face in the initial configuration, which can be solved by numerical integration. In order to validate the theoretical model, the results of the ballistic limits as well as the residual velocities were compared to the experimental and the numerical model results. Agreement between theoretical model and experimental and FE results was found, with a maximum difference lower than 10%.

Two representative Π groups are studied to assess the physical consistency of the model. These results suggest that the ballistic response is governed by the laminate/projectile and the laminate Young's modulus E_{11}.

The FE model was used to validate some of the hypotheses of the theoretical model. Overall, the predictions of relative displacement or penetration, $\bar{\delta}$, by both models are in good agreement. The most critical cases, when full penetration does not occur, present small differences in the predictions for both thicknesses.

This agreement becomes worse when increasing the laminate thicknesses, as its structural response experiences a transition from thin to thick laminate. For thin laminates, changing the projectile shape leads to the same ballistic results if diameter and mass are maintained. However, the relative contribution of the energy absorption mechanisms/failure modes may change with projectile geometry.

The failure mechanisms in the numerical model are associated to the different energy-absorption mechanisms considered in the theoretical model. Energy-absorption mechanisms are compared between the theoretical and the FE models for three ballistic regimes: below, above and at the ballistic limit for for 3 mm and 6 mm laminates. Fibre failure is identified as the most important energy-absorption mechanism while matrix cracking and delamination are proved to play a minor role. Out-of-plane failure mechanisms such as compression and shear plugging are more important at high-impact velocities and for 6 mm laminates, which are close to the thick behaviour.

6. Acknowledgements

L. Alonso, S.K.García Castillo and C.Navarro are indebted to the project 'Acción Estratégica en Materiales Compuestos y Análisis Numérico simplificado de Estructuras y protecciones ligeras sometidas a impacto balístico' (2010/00309/002) of the University Carlos III of Madrid for the financial support of this work. D. Garcia-Gonzalez acknowledges support from the Talent Attraction grant (CM 2018 - 2018-T2/IND-9992) from the Comunidad de Madrid. F. Martínez-Hergueta acknowledges support from PECRE1819_02 from the Scottish Research Partnership in Engineering.

References

Abaqus6.14, 2014. Systemes D. Abaqus 6.14 User's manual.

Alonso, L., Martínez-Hergueta, F., Garcia-Gonzalez, D., Navarro, C., García-Castillo, S., Teixeira-Dias, F., 2020. A finite element approach to model high-velocity impact on thin woven gfrp plates. International Journal of Impact Engineering 142. doi:doi:10.1016/j.ijimpeng.2020.103593.

Alonso, L., Navarro, C., García-Castillo, S., 2018a. Analytical models for the perforation of thick and thin thicknesses woven-laminates subjected to high-velocity impact. Composites Part B 143, 292–300. doi:doi:10.1016/j.compositesb.2018.01.030.

Alonso, L., Navarro, C., García-Castillo, S., 2018b. Experimental study of woven-laminates structures subjected to high-velocity impact. Mechanics of Advanced Materials and Structures doi:doi:10.1080/15376494.2018.1526354.

Briescani, L., Manes, A., Giglio, M., 2015. An analytical model for ballistic impacts against plain-woven fabrics with a polymeric matrix. International Journal of Impact Engineering 78, 138–149. doi:doi:10.1016/j.ijimpeng.2015.01.001.

Buitrago-Pérez, B., García-Castillo, S., Barbero, E., 2010. Experimental analysis of perforation of glass/polyester structures subjected to high-velocity impact. Material Letters 64, 1052–1054. doi:doi:10.1016/j.matlet.2010.02.007.

Cantwell, W., Morton, J., 1990. Impact perforation of carbon fibre reinforced plastic. Composite Science and Technology 38, 119–141. doi:doi:10.1016/0266-3538(90)90002-M.

Chang, F., Chang, K., 1987. A progressive damage model for laminated composites containing stress concentrations. Journal of Composite Materials 21, 834–855. doi:doi:10.1177/002199838702100904.

García-Castillo, S., López-Puente, J., Sánchez Sáez, S., Barbero, E., Navarro, C., 2006. Analytical model for energy absorption capabilities of glass/polyester panels subjected to ballistic impact. Conference in Developments in Theoretical and Applied Mechanics .

García-Castillo, S., Sánchez Sáez, S., López-Puente, J., Barbero, E., Navarro, C., 2009. Impact behaviour of preloaded glass/polyester woven plates. Composites Science and Technology 69, 711–717. doi:doi:10.1016/j.compscitech.2008.01.007.

García-Castillo, S., Sánchez Sáez, S., Santiuste, C., Barbero, E., Navarro, C., 2013. Perforation of Composite Laminate Subjected to Dynamic Loads. Springer Netherlands. pp. 291–337. doi:doi:10.1007/978-94-007-5329-7_7.

Gellert, E., Cimpoeru, S., R.L., W., 2000. A study of the effect of target thickness on the ballistic perforation of glass-fibre-reinforced plastic composites. International Journal of Impact Engineering 24, 445–456. doi:doi:10.1016/S0734-743X(99)00175-X.

Gil-Alba, R., Alonso, L., Navarro, C., García-Castillo, S., 2019. Morphological study of damage evolution in woven-laminates subjected to high-velocity impact. Mechanics of Advanced Materials and Structures doi:doi:10.1080/15376494.2019.1692264.

Gregori, D., Scazzosi, R., Nunes, S., Amico, S., Giglio, M., Manes, A., 2020. Analytical and numerical modelling of high-velocity impact on multilayer alumina/aramid fiber composite ballistic shields: Improvement in modelling approaches. Composites Part B 187. doi:doi:10.1016/j.compositesb.2020.107830.

Harding, J., Ruiz, C., 1998. The mechanical behaviour of composite materials under impact loading. Key Engineering Materials 141-143, 403–426. doi:doi:10.4028/www.scientific.net/KEM.141-143.403.

Harding, J., Welsh, L., 1983. A tensile testing technique for fiber-reinforced composites at impact rates of strain. Journal of Material Science 18, 1810–1826. doi:doi:10.1007/BF00542078.

Hashin, Z., 1980. Failure criteria for unidirectional fiber composites. Journal of Applied Mechanics 47, 329–334. doi:doi:10.1115/1.3153664.

Kenane, M., Benzeggagh, M., 1997. Mixed-mode delamination fracture thoughness of unidirectional glass/epoxi composites under fatigue loading. Composites Science and Technology 57, 597–605. doi:doi:10.1016/S0266-3538(97)00021-3.

Kim, H., Welch, D., Kedward, K., 2003. Experimental investigation of high velocity ice impacts on woven carbon/epoxi composite panels. Composites Part A 34, 25–41. doi:doi:10.1016/S1359-835X(02)00258-0.

Lambert, J., Jonas, G., 1976. Towards standarization of in terminal ballistic testing: velocity representation. Ballistic research laboratories .

Llorca, J., González, C., Molina-Aldareguía, J.M., Segurado, J., Seltzer, R., Sket, F., Rodríguez, M., Sádaba, S., Muñoz, R., Canal, L.P., 2011. Multiscale modeling of composite materials: a roadmap towards virtual testing. Advanced Materials 23, 5130–5147.

López-Puente, J., Zaera, R., Navarro, C., 2007. An analytical model for high velocity impact on thin cfrps woven laminated plates. International Journal of Solids and Structures 44, 2837–2851. doi:doi:10.1016/j.ijsolstr.2006.08.022.

Mamivand, M., Liaghat, G., 2010. A model for ballistic impact on multi-layer fabric targets. International Journal of Impact Engineering 37, 806–812. doi:doi:10.1016/j.ijimpeng.2010.01.003.

Menna, C., Asprone, D., Caprino, G., Lopresto, V., Prota, A., 2011. Numerical simulation of impact tests on gfrp composite laminates. International Journal of Impact Engineering 38, 677–685. doi:doi:10.1016/j.ijimpeng.2011.03.003.

Miamí, P., Camanho, P., Mayugo, J., Dávila, C., 2007. A continuum damage model for composite laminates: Part ii–computational implementation and validation. Mechanics of Materials 39, 909–919. doi:doi:10.1016/j.mechmat.2007.03.006.

Mohotti, D., Ngo, T., Raman, S., Mendis, P., 2015. Analytical and numerical investigation of polyurea layered aluminium plates subjected to high velocity projectile impact. Materials & Design 82, 1–17. doi:doi:10.1016/j.matdes.2015.05.036.

Moyre, S., Hine, P., Duckett, R., Carr, D., Ward, I., 2000. Modelling of the energy absorption by polymer composites upon ballistic impact. Composites Science and Technology 60, 2631–2642. doi:doi:10.1016/S0266-3538(00)00139-1.

Muñoz, R., Martínez-Hergueta, F., Gálvez, F., González, C., Llorca, J., 2015. Ballistic performance of hybrid 3d woven composites: experiments and simulations. Composite Structures 127, 141–151.

Naik, N., Doshi, A., 2005. Ballistic impact behaviour of thick composites: Analytical formulation. AIAA Journal 43, 1525–1536. doi:doi:10.2514/1.11993.

Naik, N., Shrirao, P., 2004. Composite structures under ballistic impact. Composite Structures 66, 579–590. doi:doi:10.1016/j.compstruct.2004.05.006.

Naik, N., Shrirao, P., Reddy, B., 2005. Ballistic impact behaviour of woven fabric composites: Parametric studies. Material Science & Engineering A 412, 104–116. doi:doi:10.1016/j.msea.2005.08.019.

Naik, N., Shrirao, P., Reddy, C., 2006. Ballistic impact behaviour of woven fabric composites: Formulation. Intenational Journal of Impact Engineering 32, 1521–1552. doi:doi:10.1016/j.ijimpeng.2005.01.004.

Navarro, C., 1998. Simplified modelling of the ballistic behaviour of fabric and fibre-reinforced polymer matrix composites. Key Engineering Materials 141–143, 383–400.

Rhymer, J., Kim, H., Roach, D., 2012. The damage resistance of quasi-isotropic carbon/epoxy composite tape laminates impacted by high velocity ice. Composites Part A: Applied Science and Manufacturing 43, 1134–1144. doi:doi:10.1016/j.compositesa.2012.02.017.

Smith, J., F.L., M., Schiefer, H., 1958. Stress-strain relationships in yarns subjected to rapid impact loading:5. wave propagation in long textile yarns impacted transversally. Journal of Research of National Bureau of Standars 60, 517–534.

Turon, A., Dávila, C., Camaho, P., Coste, J., 2007. An engineering solution for mesh size effects in the simulation of delamination using cohesive zone models. Engineering Fracture Mechanics 74, 1665–1682. doi:doi:10.1016/j.engfracmech.2006.08.025.

Ulven, C., Vaidya, U., Hosur, M., 2003. Effect of projectile shape during ballistic perforation of vartm carbon/epoxy composite panels. Composite Structures 61, 143–150. doi:doi:10.1016/S0263-8223(03)00037-0.

Wen, H., 2000. Predicting the penetration and perforation of frp laminates struck normally by projectiles with different nose shapes. Composite Structures 49, 321–329. doi:doi:10.1016/S0263-8223(00)00064-7.

Wen, H., 2001. Penetration and perforation of thick fpr laminates. Composite Science and Technology 51, 1163–1172. doi:doi:10.1016/S0266-3538(01)00020-3.

Xiao, J., Gama, B., Gillespie Jr, J., 2007. Progressive damage and delamination in plain weave s-2 glass/sc-15 composites under quasi-static punch-shear loading. Composite Structures 78, 182–196. doi:doi:10.1016/j.compstruct.2005.09.001.

Zhu, G., Goldsmith, W., Dharan, C., 1992. Penetration of laminated kevlar by projectiles ii. analytical model. International Journal of Solids and Structures 29, 421–436. doi:doi:doi.org/10.1016/0020-7683(92)90208-B.